

CANCER

Direct measurement of vertical forces shows correlation between mechanical activity and proteolytic ability of invadopodia

E. Dalaka¹, N. M. Kronenberg¹, P. Liehm¹, J. E. Segall², M. B. Prystowsky², M. C. Gather^{1*}

Mechanobiology plays a prominent role in cancer invasion and metastasis. The ability of a cancer to degrade extracellular matrix (ECM) is likely connected to its invasiveness. Many cancer cells form invadopodia—micrometer-sized cellular protrusions that promote invasion through matrix degradation (proteolysis). Although it has been hypothesized that invadopodia exert mechanical force that is implicated in cancer invasion, direct measurements remain elusive. Here, we use a recently developed interferometric force imaging technique that provides piconewton resolution to quantify invadopodial forces in cells of head and neck squamous carcinoma and to monitor their temporal dynamics. We compare the force exerted by individual protrusions to their ability to degrade ECM and investigate the mechanical effects of inhibiting invadopodia through overexpression of microRNA-375. By connecting the biophysical and biochemical characteristics of invadopodia, our study provides a new perspective on cancer invasion that, in the future, may help to identify biomechanical targets for cancer therapy.

INTRODUCTION

Cellular forces are crucial for the coordination of many cellular processes, including cancer progression, invasion, and metastasis (1–3). The compliance of cells and of the surrounding extracellular matrix (ECM) and the mechanical action of cells on their surroundings all contribute to the malignant phenotype, e.g., via changes of cellular conformation and regulation of invasive and metastatic behavior. Of particular importance for the invasiveness of a cancer is its ability to degrade the ECM (4). Many types of cancer cells form invadopodia, specialized actin-rich protrusions to the cell membrane that are capable of ECM degradation (5, 6). It has been hypothesized but not demonstrated that invadopodia exert mechanical force and that this force is implicated in cancer invasion (7).

The formation and activity of invadopodia include precursor assembly, anchoring, and maturation, the latter of which is accompanied by ECM degradation (8, 9). Several proteins are involved in invadopodia formation, including actin, cortactin, and the tyrosine kinase adaptor proteins Tks5 and Tks4. The main invadopodium core consists of actin filaments; cortactin binds directly to these filaments and promotes key invadopodium functions, such as initiation, formation, and proteolytic behavior (10, 11). Tks5 is essential for invadopodium formation and stability but not for matrix degradation, whereas Tks4 regulates the formation of invadopodial protrusions (12). ECM degradation occurs, at least in part, through the release of different matrix metalloproteases (MMPs), including membrane type 1 (MT1)–MMP, MMP-2, and MMP-9 (13).

Mechanical stimulation of cells has been correlated with higher numbers and enhanced proteolytic activity of invadopodia (14). There is also evidence that invadopodia protrude into their substrate in a dynamic, oscillatory way by actin polymerization (15) and possibly by actomyosin contractility (16) and that they perform local mechanosensing through the biochemical activity of integrins (17). Whole-cell contractility, measured via traction force microscopy (TFM), has been correlated with invadopodial activity to assess the

metastatic ability of cells (18, 19). However, direct observation and measurement of forces exerted by individual invadopodia remain elusive, with evidence for the existence of a mechanical force limited to the observation of nuclear indentations caused by invadopodia that are located between the ventral cell membrane and the nucleus (20).

A number of nonmalignant cells, including macrophages and endothelial cells, form processes known as podosomes, which are structurally and functionally related to invadopodia. Using either a modified form of atomic force microscopy (AFM) or elastic resonator interference stress microscopy (ERISM; see below), it was shown that podosomes exert dynamic vertical forces against the cell substrate that lead to an oscillatory protrusive behavior (21–25). Compared to podosomes, invadopodia are smaller in size, occur in lower numbers per cell (typically <20), and show a lower rate of turnover (26). Invadopodia generally form irregular patterns underneath the nucleus, while podosomes tend to arrange in more ordered, ring-shaped structures. This difference suggests that invadopodia can achieve mechanical support for protrusion via pushing against the cellular nucleus, while podosomes are directly linked to the actin cloud. The specific localization of invadopodia within the cell may also be functionally linked to the requirement to translocate the nucleus in a dense ECM (27). Yet, the question arises whether the degrading behavior of invadopodia is connected to a particular mechanical phenotype and whether ECM degradation is mechanically assisted.

Conventional stress microscopy techniques, such as TFM, generally reach at best a vertical stress sensitivity and spatial resolution of 50 Pa and 2 μm , respectively (28–31), and thus are unlikely to allow observation of the force exerted by individual invadopodia. Our recently introduced ERISM method monitors cell forces with high spatial resolution and unprecedented sensitivity to vertical forces, resolving vertical deformations of 2 nm, stresses of 1 Pa, and—for localized indentations—forces of ≈ 1 pN (23, 32). This is achieved by growing cells on an optical microcavity substrate that consists of a layer of an ultrasoft elastomer that is situated between two semitransparent, mechanically flexible gold mirrors, the upper of which is coated with ECM proteins. Mechanical forces exerted by cells cause local deformations of the microcavity and, thus, local shifts to its resonance wavelengths. The resulting interference patterns are analyzed by

Copyright © 2020
The Authors, some
rights reserved;
exclusive licensee
American Association
for the Advancement
of Science. No claim to
original U.S. Government
Works. Distributed
under a Creative
Commons Attribution
License 4.0 (CC BY).

¹SUPA, School of Physics and Astronomy, University of St Andrews, St Andrews, UK.

²Albert Einstein College of Medicine, Bronx, NY 10461, USA.

*Corresponding author. Email: mcg6@st-andrews.ac.uk

optical and subsequent mechanical modeling to compute a high-resolution stress map. Unlike many other stress microscopy techniques, ERISM does not require a zero-stress reference image, allowing the experimenter to keep cells on the substrate for time-lapse imaging and immunostaining.

Here, we report the direct observation and quantification of invadopodial forces. By combining ERISM with a degradation assay, we compared the forces exerted by invadopodia to their proteolytic activity, i.e., ability to degrade ECM. Immunostaining was used to ascertain that the investigated structures are invadopodia. In addition, by studying the temporal evolution of invadopodial forces, we found an oscillatory protruding behavior with two characteristic time scales. Interfering with invadopodial protrusions by overexpression of the microRNA-375 (miR-375) resulted in reduced invadopodia force and impaired dynamics, indicating possible routes to target invadopodia-mediated cancer invasion.

RESULTS

Measurement of mechanical forces exerted by invadopodia

Our studies used the UM-SCC-1 cell line, which was derived from head and neck squamous carcinoma (HNSCC) (33, 34). HNSCC is an aggressive cancer that develops at the epithelial cell layer of the upper aerodigestive tract and is characterized by poor patient prognosis and low survival rates (35, 36). Figure 1A shows a schematic of a UM-SCC-1 cell plated on an ERISM microcavity coated with collagen or fluorescent gelatin, illustrating how invadopodia may generate protrusions, exert force, and, thus, indent the ERISM microcavity, and how—depending on the amount of indentation—light of different wavelengths fulfills the resonance condition within the microcavity. Mature invadopodia are expected to degrade the underlying collagen or gelatin matrix, while immature invadopodia may still exert mechanical force even in the absence of matrix degradation. The ERISM substrates used in this work had an effective stiffness of 3 to 4 kPa (fig. S1), similar to the typical stiffness of tissue surrounding HNSCCs (37, 38).

UM-SCC-1 cells attached well on collagen-coated ERISM substrates (Fig. 1B). Under illumination with monochromatic light, ERISM substrates showed a characteristic interference pattern, with large-scale features that map out the outer contour of the cell and typically 5 to 10 smaller-scale features underneath the cell (Fig. 1C). To quantify the deformation and stress associated with these features, we imaged the microcavity under illumination with monochromatic light of a range of different wavelengths and extracted the local deformation of the microcavity from these images via optical modeling (Fig. 1D). This revealed a broad indentation across the cell body and upward pulling along the cell periphery, a feature that has previously been associated with the presence of contractile forces, which are transmitted via focal adhesions (23). Superimposed on the broad indentation are local protrusions with a depth of approximately 6 nm. The deformation map was translated into a stress map via finite element modeling (Fig. 1E), and spatial Fourier filtering was applied to eliminate the unspecific stress from focal adhesions and overall cell contractility (Fig. 1F). This showed that the small protrusions are associated with local points of downward pushing. Integrating the stress over the area of each protrusion yielded a force of 2 to 10 pN per protrusion (see below for statistical analysis). Comparing the lateral stress profile along protrusions to background fluctuations in stress away from the cell shows that the recorded stress is well above the noise floor of the measurement (Fig. 1G).

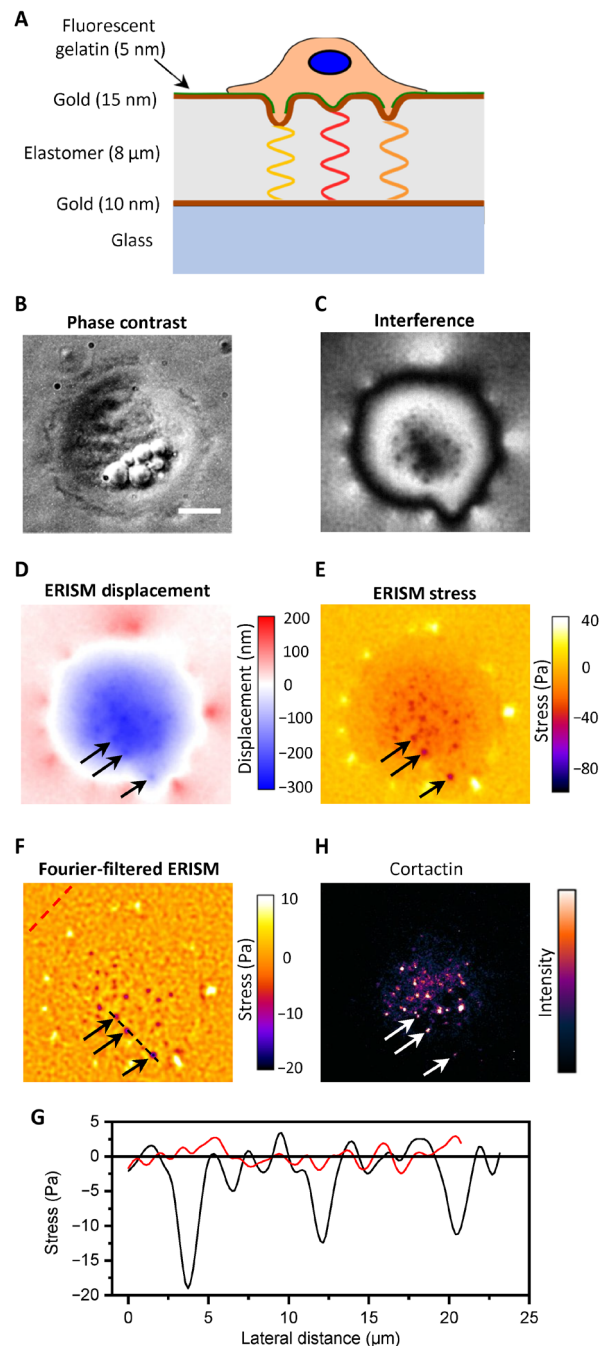


Fig. 1. ERISM for measuring the mechanical activity of invadopodia formed by UM-SCC-1 cancer cells. (A) Schematic sketch of the ERISM measurement, illustrating how invadopodia forces against an elastic microcavity, formed by two gold films sandwiching a soft elastomer, lead to local changes in the thickness and resonance wavelengths of the microcavity. The microcavity substrate is coated with fluorescent gelatin (green line) to distinguish mature (degrading) from immature (nondegrading) invadopodia. (B) Phase-contrast image of UM-SCC-1 cell attached to the microcavity surface. (C) Coregistered monochromatic reflectance image of the microcavity, for illumination with 676-nm light. (D) ERISM thickness map obtained from a series of reflectance images, showing the substrate deformation induced by the same cell. Black arrows indicate three local indentation features. (E) ERISM stress map and (F) ERISM stress map after application of Fourier band-pass filter. (G) Lateral stress profile along the black and red dashed lines in (F). (H) Epifluorescence image of the same cell after immunostaining for cortactin. Scale bar, 10 μm .

To test whether the protrusive structures imaged with ERISM were due to invadopodial activity, we stained for actin and the invadopodia marker cortactin (Fig. 1H and fig. S2). Most protrusions correlated with actin and cortactin staining, corroborating that these result from invadopodia. We have previously found that the characteristic cortactin dots observed here colocalize fully with the invadopodia marker Tks5 (34), which we take as additional evidence that the observed protrusions are caused by invadopodia. Colocalization of cortactin, Tks5, and protrusive events was also confirmed for one example of cells on an ERISM substrate (fig. S2). Some cortactin puncta did not show a corresponding indentation. These nonindenting cortactin dots may be associated with early cortactin recruitment in developing invadopodial structures, i.e., with precursor assembly (39).

Correlation of invadopodial force with ECM degradation

Not all invadopodia formed by a cancer cell become mature, i.e., are able to degrade the ECM. To explore the forces exerted by mature and immature invadopodia separately, we determined invadopodial maturity with an accepted degradation assay that is based on a fluorescent gelatin layer that only mature invadopodia are able to degrade (34). In the literature, immunostaining for MT1-MMP is described as an alternative way to distinguish mature and immature invadopodia. Both assays provide similar results (9), and we opted for the fluorescent gelatin assay as this does not require fixation of cells and, thus, offers better compatibility with the live force imaging capability of ERISM. The ERISM substrate was coated with a thin film of fluorescent gelatin (thickness measured with AFM, 5.5 ± 1.2 nm), which did not cause a change in microcavity stiffness (fig. S1). Cells adhered well to the ERISM substrate (Fig. 2, A and B) and again showed the localized protrusions we previously associated with invadopodia activity (Fig. 2, C and D). Gelatin fluorescence was strongly decreased in some, but not all, of these tightly localized spots (Fig. 2, E and F), consistent with some

invadopodia entering their maturation stage and degrading the matrix. Protrusions on ERISM maps that were colocalized with areas of degraded matrix were labeled as mature invadopodia, while protrusions without associated matrix degradation were classified as immature. We analyzed 14 cells and a total of 158 invadopodia, 66 of which were classified as mature (data from three independent experiments). Mature invadopodia exerted significantly larger forces than immature ones (median force \pm SEM, $F_{\text{mat}} = 5.8 \pm 0.4$ pN, $F_{\text{imat}} = 3.4 \pm 0.4$ pN, $P = 0.0008$, Mann-Whitney U test; Fig. 2G). These data indicate that invadopodial force generation may play a role in ECM degradation, possibly supporting the enzymatic activity of MMPs (fig. S3). Comparing the forces exerted by mature and immature invadopodia at different time points, we found that at the single-cell level, only mature invadopodia become stronger as time evolves (fig. S4).

Invadopodia exert highly dynamic and oscillatory forces

Invadopodia are dynamic structures, typically showing turnover within 5 to 15 min (40, 41). ERISM force measurements allowed us to study the temporal dynamics of the mechanical activity of invadopodia and to correlate them with their degradative ability. We followed the periodic protrusions of invadopodia into the substrate, using ERISM time-lapse force imaging of UM-SCC-1 cells (Fig. 3, A to C, and movies S1 and S2). From these data, we extracted the temporal evolution of the force exerted by a single invadopodium (Fig. 3D and fig. S5; a reference trace from a region not containing invadopodia corroborates that the observed changes in force are well above the noise floor of the measurement).

To analyze this behavior in more detail, we followed and analyzed the force generated by 93 invadopodia (from five different cells and three individual experiments) over the course of several hours, with data recorded every 10 s. This revealed a two-mode oscillatory behavior; on average, invadopodia showed cycles of high mechanical

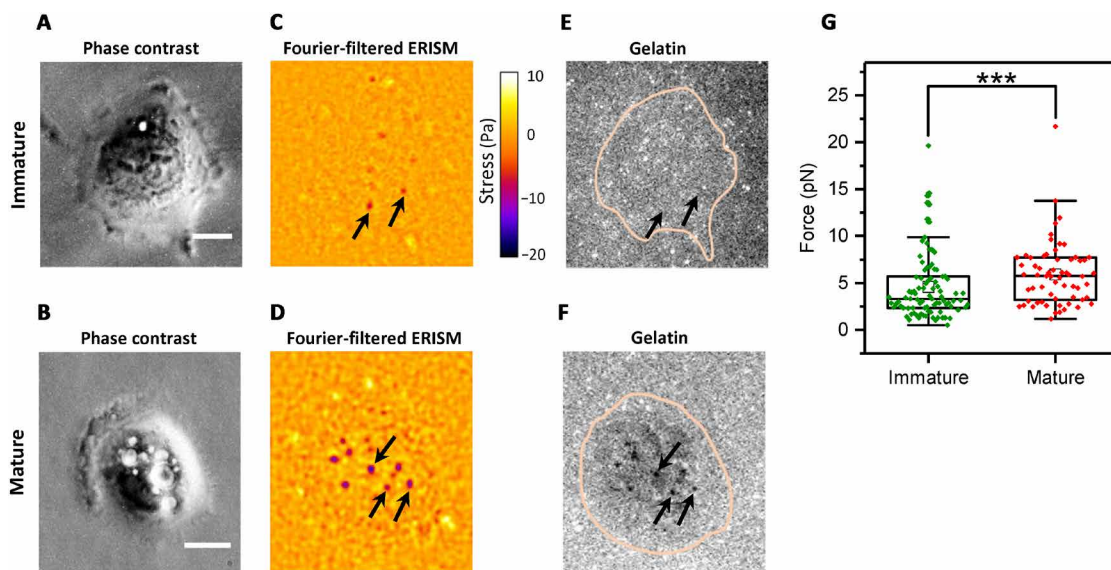


Fig. 2. Correlation of invadopodial force with matrix degradation. (A and B) Phase-contrast images of two representative UM-SCC-1 cells with immature and mature invadopodia, respectively. (C and D) Fourier-filtered ERISM stress map of same cells, with arrows indicating representative invadopodia in each cell. (E and F) Epifluorescence image of fluorescent gelatin film on the surface of the ERISM substrate. Pink lines indicate the outline of cells. The maturity of invadopodia was classified by analysis of local gelatin fluorescence. (G) Comparison between force exerted by mature ($n = 66$) and immature ($n = 92$) invadopodia. Each data point represents the mean force exerted by an invadopodium over a 1-hour time frame. Plots indicate data (diamonds), median (center), mean (open square), Q1/Q3 (box), and ± 1.5 SD (whiskers). As data in groups were not normally distributed, groups were compared using the Mann-Whitney U test (***) ($P < 0.001$). Scale bars, 10 μ m.

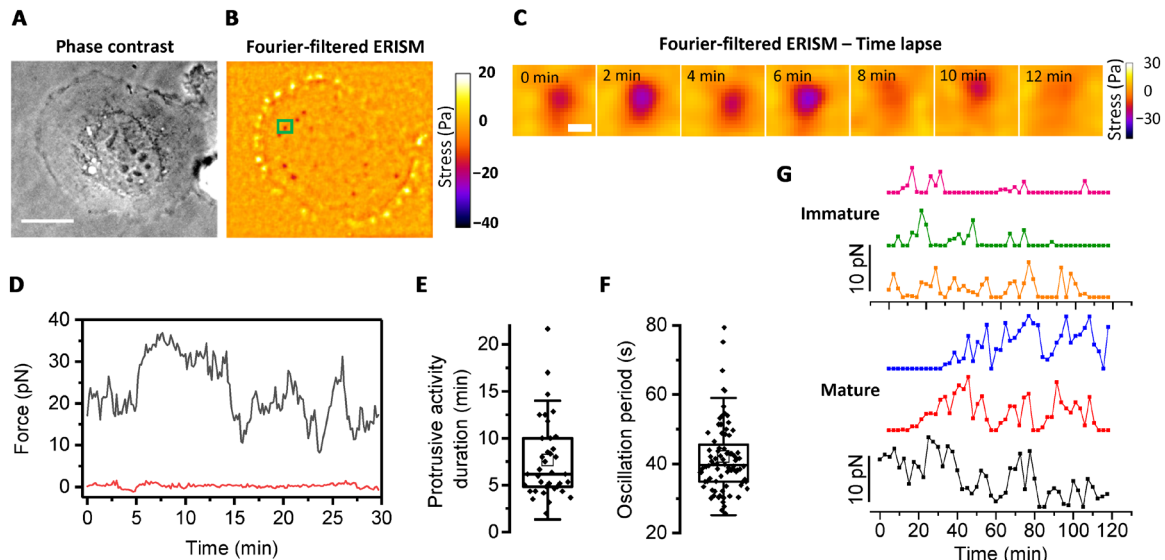


Fig. 3. Dynamics of mechanical activity of invadopodia. (A) Phase-contrast image and (B) Fourier-filtered ERISM stress map of a typical UM-SCC-1 cell. (C) Time lapse of the invadopodium indicated by the green rectangle in (B), imaged every 2 min. (D) Temporal evolution of force exerted by a single invadopodium (gray line) and background force in a region without invadopodia (red line). Force measurements were taken every 10 s; recording started 2 hours after cell seeding. (E) Overall duration of protrusive activity and (F) mean duration of fast oscillation cycles in force for multiple invadopodia (3 individual experiments, 5 cells, and 93 invadopodia, of which 45 were classified as mature, 8 as immature, and the remaining not classified). Plots indicate data (diamonds), median (center), mean (open square), Q1/Q3 (box), and ± 1.5 SD (whiskers). (G) Time evolution of forces exerted by three immature (top) and three mature (bottom) invadopodia. Force measurements were taken every 2.5 min; recording started 3 hours after cell seeding. Scale bars, 20 μm (A) and 1 μm (C).

activity lasting 7.2 ± 4.1 min (Fig. 3E) and, in addition, exhibited a fast oscillation in force with a characteristic period of 43.3 ± 1.7 s (Fig. 3F and fig. S6). This two-mode behavior may reflect a combination of a periodic exertion of mechanical force supporting matrix degradation (slow force variation), accompanied by a faster oscillation. Similar dynamics, i.e., a combination of fast and slow oscillations, have also been observed when mapping stiffness changes of podosome protrusions using AFM (22). Comparing the force dynamics of invadopodia with their degrading ability showed that mature invadopodia were more active and persisted for a longer time span than immature invadopodia (Fig. 3G and movies S1 and S2). Combined with our earlier observation of larger forces in mature invadopodia, this observation suggests a link between successful ECM degradation and the presence of persistent and oscillatory forces.

miR-375 overexpression affects invadopodia mechanics

miRNAs are small, noncoding strands of RNA, which regulate gene expression in health and malignancy and behave as oncogenes or cancer suppressors. Previous work has shown that low-level expression of miR-375 enhances cancer invasiveness and is associated with poor patient outcome (33); conversely, overexpression of miR-375 can suppress invadopodia maturation and reduce cancer invasiveness (34). Here, we investigated the effect of miR-375 overexpression on the mechanical activity of UM-SCC-1 cells.

Control and miR-375-overexpressing UM-SCC-1 cells showed comparable morphology (Fig. 4, A and B). Likewise, the broad indentation across the cell body and the upward pulling along the cell periphery were comparable (Fig. 4, C and D). However, after filtering out the broad indentation using spatial Fourier filtering as described before, we found that miR-375 overexpression led to a significant change in the mechanical activity of individual invadopodia with fewer and weaker invadopodia (Fig. 4, E and F). To quantify the

effect of miR-375 overexpression on mechanical activity, we first calculated the total volume by which cells indent into the substrate, which provides a measure of the overall contractile force generated by the whole cell (Fig. 4G). This showed no significant difference between the two cell populations. However, the number of indenting invadopodia per cell in miR-375-overexpressing cells decreased significantly (Fig. 4H), and the force exerted by the remaining invadopodia became significantly smaller (Fig. 4I). Earlier findings showed that overexpression of miR-375 in UM-SCC-1 cells decreases the proteolytic behavior of these cells, i.e., fewer invadopodia and less invasion, but that the remaining invadopodia stained positively for Tks5 and that some invadopodia retained degrading ability (34). Our experiments now show that miR-375 overexpression also compromises invadopodia mechanics, consistent with a block in invadopodia maturation.

DISCUSSION

On the basis of the results of our investigation, we propose a mechanical model for invadopodia-mediated cancer invasion. Formation of an invadopodium is followed by actin polymerization in the main invadopodium core, which then leads to a protrusion at the ventral part of the cell membrane (42). These protrusions exert piconewton pushing forces, i.e., forces that are directed perpendicular and outward with respect to the cell membrane. Mature (degrading) invadopodia apply, on average, significantly higher forces than immature (nondegrading) ones.

There is increasing interest in the temporal dynamics of cell forces, e.g., to understand whether and how mechanical aspects regulate cell cycle progression (43). Our work now shows that invadopodial forces are also highly dynamic with fluctuations on two distinct time scales; they exert a vertical downward force about every 7 min, which is accompanied by faster variations in force approximately every 40 s. We hypothesize that the slow component of the dynamics

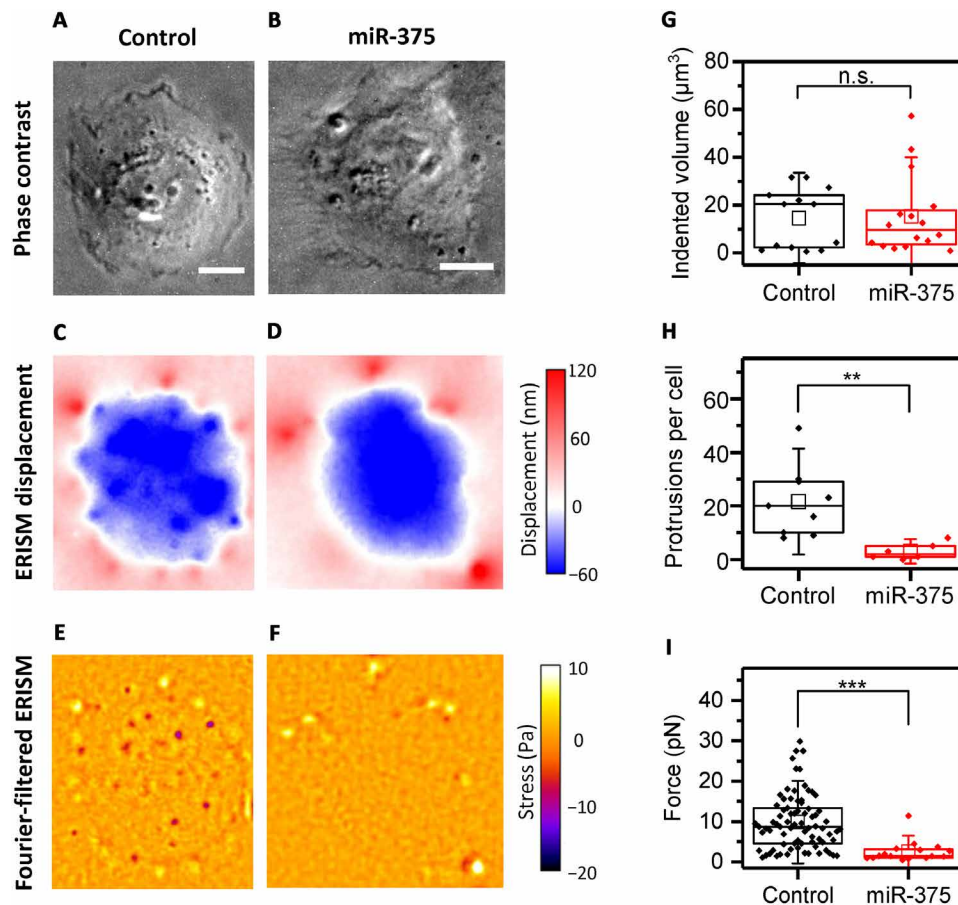


Fig. 4. Impact of overexpression of the miR-375 on the mechanical activity of UM-SCC-1 cells. (A and B) Phase-contrast, (C and D) ERISM, and (E and F) Fourier-filtered ERISM images of representative UM-SCC-1 control cell (left column) and miR-375-overexpressing cell (right column). (G) Comparison of total volume by which cells indent into the ERISM substrate. Control, $n = 13$ cells; miR-375, $n = 16$ cells. As data in groups were not normally distributed, groups were compared using the Mann-Whitney U test ($P = 0.983$). (H) Comparison of the number of protruding invadopodia formed per cell (mixed population of mature and immature invadopodia). Control, $n = 9$ cells; miR-375, $n = 6$ cells. Two-sample t test ($P = 0.005$). (I) Comparison of force exerted by invadopodia from both cell types. Control, $n = 106$ invadopodia from eight cells; miR-375, $n = 47$ invadopodia from three cells. As data in groups were not normally distributed, groups were compared using the Mann-Whitney U test ($P = 1.41 \times 10^{-6}$). Statistical tests: not significant (n.s.), $P > 0.05$; ** $P < 0.01$; *** $P < 0.001$. Scale bars, 20 μm .

is associated with actin polymerization at the invadopodium core, which, after a few minutes, reaches its maximum length, causing the invadopodium to collapse and actin monomers to be released back into the cytoplasm, thereby triggering a new cycle of actin polymerization and, thus, invadopodium formation (40, 41). The faster force fluctuations may instead be due to treadmilling of actin filaments at the invadopodium core (44) and could be associated with mechanosensing and membrane tension (45–48).

Invadopodial forces are more dynamic and persistent in mature invadopodia, suggesting that the protrusive activity (i.e., the slow force component) contributes to matrix degradation and to breaking of the ECM barrier. Protrusion force could expose sites in the ECM that could be remodeled or bring membrane-associated proteases such as MT1-MMP into close contact with ECM substrates, resulting in efficient matrix degradation and cancer invasion. The difference in force exerted by mature and immature invadopodia further suggests that there may be a minimum threshold force for invadopodia to achieve ECM degradation.

In agreement with earlier studies, we observed that overexpression of miR-375 significantly decreases the number of invadopodia

(33, 34). However, in addition, we found that the forces generated by the few surviving invadopodia were markedly decreased but that mechanical activity and contractility on the level of the whole cell were not affected. This indicates that miR-375 overexpression specifically impairs the formation and function of invadopodia, thus providing a potential avenue for reducing invadopodia-mediated invasion and metastasis in cancer therapy.

In the future, studying the effect of external mechanical and chemical signals on invadopodial force is likely to improve our understanding of invadopodia-mediated cancer invasion. On the basis of our observations and measurements, future studies should attempt to further elucidate the connection between mechanical forces exerted by invadopodia and their ability for ECM degradation, particularly to establish if there is a causal link and a defined timing of events, i.e., if force precedes or follows ECM degradation. It will also be interesting to study the mechanical activity and proteolytic ability upon silencing, overexpression, or mutation of invadopodia-associated proteins, such as cortactin or MMPs. In addition, ERISM may provide new insights into the role of invadopodia in cell adhesion, which is believed to play a crucial role in cancer. The invadopodium core is

surrounded by adhesion proteins (e.g., paxillin and vinculin), which create a ring-like structure around the main actin core (49), and it is tempting to speculate that this adhesive structure exerts forces that counterbalance the protrusion of the invadopodium core or influence the mechanical activity of invadopodia in other ways.

MATERIALS AND METHODS

Cell lines and cell cultures

Cells of the HNSCC cell line UM-SCC-1 and a previously developed derivative, in which the miR-375 is overexpressed (33), were provided by T. Carey from the University of Michigan. Cells were cultured in Dulbecco's modified Eagle's medium (DMEM; high glucose, GlutaMAX-I, Gibco 61965-026) fortified with 10 volume % fetal bovine serum (Biosera FB-1001), 1 volume % minimum essential medium, nonessential amino acids (100×, Gibco 11140-035), and 1 volume % penicillin-streptomycin (Gibco 15140122). For epifluorescence microscopy, phenol red-free DMEM (Gibco 31053-028) with 1 volume % GlutaMAX-I was used.

ERISM substrates were fabricated as described previously (23). The substrate surface was separated into smaller compartments by mounting 7.5×7.5 -mm² silicone chambers on the ERISM substrate (obtained by cutting down removable 12-well chambers; Ibidi 81201), and 3000 cells were plated in each chamber.

Collagen-I coating

Collagen-I (1 mg/ml; Millipore L7220) was mixed with low-pH phosphate-buffered saline (PBS) (pH 3.0 to 3.5) in a 1:1 ratio, at a total volume of 350 μ l for each silicone chamber. The mixture was applied to the ERISM substrate and incubated for 30 min at 37°C and 5% CO₂. The substrate was then washed three times with PBS (pH 7.4) and twice with cell culture medium.

Gelatin coating

Gelatin coatings on ERISM substrates were prepared using a commercial assay (Millipore ECM670) following the manufacturer's instructions, except that during the washing steps, the ERISM substrate was not allowed to fall completely dry to prevent damage to the surface. To still ensure complete removal of the previous reagent, the number of washing steps was increased from 3 to 6. Moreover, the chamber was washed twice with each reagent before incubation to minimize dilution of the reagent by the previously present liquid. The thickness of the gelatin coating on gold was determined with an AFM (Nanosurf, FlexAFM).

Immunostaining

Cells were fixed directly on the ERISM substrate with 4% formaldehyde (formaldehyde 37%, Millipore 1.04003.1000) in PBS for 20 min, washed twice with 0.05% Tween 20 (diluted from Alfa Aesar J63596; all washing steps involved a 5-min incubation at room temperature, unless noted otherwise), and permeabilized with 0.05% Triton X-100 (Alfa Aesar A16046). After again washing twice with 0.05% Tween 20, cells were blocked with 1% bovine serum albumin (BSA; Albumin Fraction V, >98%; Roth 80761) in PBS for 30 min, incubated with a primary anticortactin antibody (1 mg/ml; Millipore 05-180; 1:100 dilution in 1% BSA) or anti-Tks5 antibody [fish (M-300), 200 μ g/ml; Santa Cruz Biotechnology sc-30122; 1:50 dilution in 1% BSA) at room temperature for 1 hour, washed three times in 0.05% Tween 20 and twice with 1% BSA, and then incubated with a secondary Cy3 anti-

mouse antibody (1.5 mg/ml; Jackson ImmunoResearch Laboratories 715-165-150; 1:400 dilution in 1% BSA) and TRITC (tetramethyl rhodamine isothiocyanate)-phalloidin (EMD Millipore CS207796; 1:50 dilution in 1% BSA) or Cy5 anti-rabbit (1.5 mg/ml; Jackson ImmunoResearch Laboratories 711-175-152; 1:400 dilution in 1% BSA) at room temperature for 1 hour. Cells were again washed three times with 0.05% Tween 20 and twice with 1% BSA. Last, cells were incubated with DAPI (4',6-diamidino-2-phenylindole) (EMD Millipore 90229; 1:100 dilution in 1% BSA) at room temperature for 3 min and washed three times with 0.05% Tween 20.

Image analysis, data analysis, and statistical testing

ERISM displacement maps were generated from recorded sets of monochromatic interference images using an in-house Python code, and ERISM stress map was generated from these using finite element modeling (COMSOL Multiphysics) as described previously (23). Further image analysis was performed in ImageJ. A fast Fourier transform (FFT) filter was applied to remove unspecific broad deformations caused by focal adhesion-mediated overall contractility of the cell. FFT parameters were typically set to filter features larger than 10 pixels (1.62 μ m) and smaller than 3 pixels (0.49 μ m) from each stress map. To measure the invadopodia force or the total indented volume for an entire cell, a threshold was applied to the image, before integrating over areas of downward stress (for force) or downward deformation (for volume).

To quantify the period of fast oscillations, stress maps were acquired every 10 s, and the force exerted by the respective invadopodium was plotted over time. The time at which the local maximum in force occurred was read off, and the cumulative number of force maxima was plotted over time. The slope of a linear fit to these data then yielded the period at which fast force oscillations occurred. The mean of this value was calculated from analyzing multiple protrusions. For the slow force oscillation, the raw force data were again plotted over time for each protrusion, and the time difference between two force minima was read off. The mean of these values was calculated from analyzing multiple protrusions. Force measurements lasted 2.0 to 4.5 hours.

Statistical testing was performed with the OriginPro 2017 software (OriginLab Corp). For normally distributed data, the two-sample *t* test was applied, whereas the Mann-Whitney nonparametric test was used when the data were not normally distributed. The level of significance was set to 0.05, and the calculated *P* value was used to define the significant difference between the compared populations.

SUPPLEMENTARY MATERIALS

Supplementary material for this article is available at <http://advances.sciencemag.org/cgi/content/full/6/11/eaax6912/DC1>

Fig. S1. AFM measurement of thickness and apparent stiffness of ERISM substrate and gelatin coating.

Fig. S2. ERISM and immunostaining for actin, cortactin, and Tks5 in UM-SCC-1 cells.

Fig. S3. Simultaneous imaging of gelatin matrix degradation and invadopodia force.

Fig. S4. Time dependence of invadopodia force within a single cell.

Fig. S5. Long-term measurement of invadopodia forces.

Fig. S6. Fourier transform-based analysis of the characteristic period of force oscillation in invadopodia.

Movie S1. Temporal evolution of invadopodia force for a typical cell with immature invadopodia.

Movie S2. Temporal evolution of invadopodia force for a typical cell with predominantly mature invadopodia.

[View/request a protocol for this paper from Bio-protocol.](#)

REFERENCES AND NOTES

- J. M. Northcott, I. S. Dean, J. K. Mouw, V. M. Weaver, Feeling stress: The mechanics of cancer progression and aggression. *Front. Cell Dev. Biol.* **6**, 17 (2018).
- A. Parekh, A. M. Weaver, Regulation of cancer invasiveness by the physical extracellular matrix environment. *Cell Adh. Migr.* **3**, 288–292 (2009).
- T. W. Remmerbach, F. Wottawah, J. Dietrich, B. Lincoln, C. Wittekind, J. Guck, Oral cancer diagnosis by mechanical phenotyping. *Cancer Res.* **69**, 1728–1732 (2009).
- S. Linder, C. Wiesner, M. Himmel, Degrading devices: Invadosomes in proteolytic cell invasion. *Annu. Rev. Cell Dev. Biol.* **27**, 185–211 (2011).
- R. J. Eddy, M. D. Weidmann, V. P. Sharma, J. S. Condeelis, Tumor cell invadopodia: Invasive protrusions that orchestrate metastasis. *Trends Cell Biol.* **27**, 595–607 (2017).
- D. A. Murphy, S. A. Courtneidge, The ‘ins’ and ‘outs’ of podosomes and invadopodia: Characteristics, formation and function. *Nat. Rev. Mol. Cell Biol.* **12**, 413–426 (2011).
- C. Albiges-Rizo, O. Destaingu, B. Fourcade, E. Planus, M. R. Block, Actin machinery and mechanosensitivity in invadopodia, podosomes and focal adhesions. *J. Cell Sci.* **122**, 3037–3049 (2009).
- B. T. Beaty, J. Condeelis, Digging a little deeper: The stages of invadopodium formation and maturation. *Eur. J. Cell Biol.* **93**, 438–444 (2014).
- V. V. Artym, Y. Zhang, F. Seillier-Moisewitsch, K. M. Yamada, S. C. Mueller, Dynamic interactions of cortactin and membrane type 1 matrix metalloproteinase at invadopodia: Defining the stages of invadopodia formation and function. *Cancer Res.* **66**, 3034–3043 (2006).
- K. C. Kirkbride, B. H. Sung, S. Sinha, A. M. Weaver, Cortactin: A multifunctional regulator of cellular invasiveness. *Cell Adh. Migr.* **5**, 187–198 (2011).
- X. L. Ren, Y. D. Qiao, J. Y. Li, X. M. Li, D. Zhang, X. J. Zhang, X. H. Zhu, W. J. Zhou, J. Shi, W. Wang, W. T. Liao, Y. Q. Ding, L. Liang, Cortactin recruits FMNL2 to promote actin polymerization and endosome motility in invadopodia formation. *Cancer Lett.* **419**, 245–256 (2018).
- S. Iizuka, C. Abdullah, M. D. Buschman, B. Diaz, S. A. Courtneidge, The role of Tks adaptor proteins in invadopodia formation, growth and metastasis of melanoma. *Oncotarget* **7**, 78473–78486 (2016).
- S. Linder, G. Scita, RABGTPases in MT1-MMP trafficking and cell invasion: Physiology versus pathology. *Small GTPases* **6**, 145–152 (2015).
- A. N. Gasparski, S. Ozarkar, K. A. Beningo, Transient mechanical strain promotes the maturation of invadopodia and enhances cancer cell invasion in vitro. *J. Cell Sci.* **130**, 1965–1978 (2017).
- M. A. O. Magalhaes, D. R. Larson, C. C. Mader, J. J. Bravo-Cordero, H. Gil-Henn, M. Oser, X. Chen, A. J. Koleske, J. Condeelis, Cortactin phosphorylation regulates cell invasion through a pH-dependent pathway. *J. Cell Biol.* **195**, 903–920 (2011).
- J. L. Ouderkerk, M. Krendel, Myosin 1e is a component of the invadosome core that contributes to regulation of invadosome dynamics. *Exp. Cell Res.* **322**, 265–276 (2014).
- N. R. Alexander, K. M. Branch, A. Parekh, E. S. Clark, I. C. Iwueke, S. A. Guelcher, A. M. Weaver, Extracellular matrix rigidity promotes invadopodia activity. *Curr. Biol.* **18**, 1295–1299 (2008).
- R. J. Jerrell, A. Parekh, Cellular traction stresses mediate extracellular matrix degradation by invadopodia. *Acta Biomater.* **10**, 1886–1896 (2014).
- A. Aung, Y. N. Seo, S. Lu, Y. Wang, C. Jamora, J. C. del Álamo, S. Varghese, 3D traction stresses activate protease-dependent invasion of cancer cells. *Biophys. J.* **107**, 2528–2537 (2014).
- O.-Y. Revach, A. Weiner, K. Rechav, I. Sabanay, A. Livne, B. Geiger, Mechanical interplay between invadopodia and the nucleus in cultured cancer cells. *Sci. Rep.* **5**, 9466 (2015).
- A. Labernadie, A. Bouissou, P. Delobelle, S. Balor, R. Voituriez, A. Proag, I. Fourquaux, C. Thibault, C. Vieu, R. Poincloux, G. M. Charrière, I. Maridonneau-Parini, Protrusion force microscopy reveals oscillatory force generation and mechanosensing activity of human macrophage podosomes. *Nat. Commun.* **5**, 5343 (2014).
- A. Labernadie, C. Thibault, C. Vieu, I. Maridonneau-Parini, G. M. Charrière, Dynamics of podosome stiffness revealed by atomic force microscopy. *Proc. Natl. Acad. Sci. U.S.A.* **107**, 21016–21021 (2010).
- N. M. Kronenberg, P. Liehm, A. Steude, J. A. Knipper, J. G. Borger, G. Scarcelli, K. Franze, S. J. Powis, M. C. Gather, Long-term imaging of cellular forces with high precision by elastic resonator interference stress microscopy. *Nat. Cell Biol.* **19**, 864–872 (2017).
- P. Cervero, C. Wiesner, A. Bouissou, R. Poincloux, S. Linder, Lymphocyte-specific protein 1 regulates mechanosensory oscillation of podosomes and actin isoform-based actomyosin symmetry breaking. *Nat. Commun.* **9**, 515 (2018).
- N. B. M. Rafiq, Z. Z. Lieu, T. Jiang, C.-H. Yu, P. Matsudaira, G. E. Jones, A. D. Bershadsky, Podosome assembly is controlled by the GTPase ARF1 and its nucleotide exchange factor ARNO. *J. Cell Biol.* **216**, 181–197 (2016).
- K. M. Kedziora, T. Isogai, K. Jalink, M. Innocenti, Invadosomes—Shaping actin networks to follow mechanical cues. *Front. Biosci. (Landmark Ed.)* **21**, 1092–1117 (2016).
- K. Wolf, P. Friedl, Extracellular matrix determinants of proteolytic and non-proteolytic cell migration. *Trends Cell Biol.* **21**, 736–744 (2011).
- S. A. Maskarinec, C. Franck, D. A. Tirrell, G. Ravichandran, Quantifying cellular traction forces in three dimensions. *Proc. Natl. Acad. Sci. U.S.A.* **106**, 22108–22113 (2009).
- S. V. Plotnikov, B. Sabass, U. S. Schwarz, C. M. Waterman, High-resolution traction force microscopy. *Methods Cell Biol.* **123**, 367–394 (2014).
- S. Ghassemi, G. Meacci, S. Liu, A. A. Gondarenko, A. Mathur, P. Roca-Cusachs, M. P. Sheetz, J. Hone, Cells test substrate rigidity by local contractions on submicrometer pillars. *Proc. Natl. Acad. Sci. U.S.A.* **109**, 5328–5333 (2012).
- W. J. Polacheck, C. S. Chen, Measuring cell-generated forces: A guide to the available tools. *Nat. Methods* **13**, 415–423 (2016).
- P. Liehm, N. M. Kronenberg, M. C. Gather, Analysis of the precision, robustness, and speed of elastic resonator interference stress microscopy. *Biophys. J.* **114**, 2180–2193 (2018).
- T. Harris, L. Jimenez, N. Kawachi, J.-B. Fan, J. Chen, T. Belbin, A. Ramnauth, O. Loudig, C. E. Keller, R. Smith, M. B. Prystowsky, N. F. Schlecht, J. E. Segall, G. Childs, Low-level expression of miR-375 correlates with poor outcome and metastasis while altering the invasive properties of head and neck squamous cell carcinomas. *Am. J. Pathol.* **180**, 917–928 (2012).
- L. Jimenez, V. P. Sharma, J. Condeelis, T. Harris, T. J. Ow, M. B. Prystowsky, G. Childs, J. E. Segall, MicroRNA-375 suppresses extracellular matrix degradation and invadopodial activity in head and neck squamous cell carcinoma. *Arch. Pathol. Lab. Med.* **139**, 1349–1361 (2015).
- C. R. Leemans, P. J. F. Snijders, R. H. Brakenhoff, The molecular landscape of head and neck cancer. *Nat. Rev. Cancer* **18**, 269–282 (2018).
- R. L. Siegel, K. D. Miller, A. Jemal, Cancer statistics, 2018. *CA Cancer J. Clin.* **68**, 7–30 (2018).
- S. Cheng, S. C. Gandevia, M. Green, R. Sinkus, L. E. Bilston, Viscoelastic properties of the tongue and soft palate using MR elastography. *J. Biomech.* **44**, 450–454 (2011).
- J. Herman, Z. Sedlackova, J. Vachutka, T. Furst, R. Salzman, J. Vomacka, Shear wave elastography parameters of normal soft tissues of the neck. *Biomed. Pap. Med. Fac. Univ. Palacky Olomouc Czech. Repub.* **161**, 320–325 (2017).
- K. E. Pourfarhangi, A. Bergman, B. Gligorijevic, ECM cross-linking regulates invadopodia dynamics. *Biophys. J.* **114**, 1455–1466 (2018).
- V. P. Sharma, D. Entenberg, J. Condeelis, High-resolution live-cell imaging and time-lapse microscopy of invadopodium dynamics and tracking analysis. *Methods Mol. Biol.* **1046**, 343–357 (2013).
- L. Jimenez, S. K. Jayakar, T. J. Ow, J. E. Segall, Mechanisms of invasion in head and neck cancer. *Arch. Pathol. Lab. Med.* **139**, 1334–1348 (2015).
- M. Uroz, S. Wistorf, X. Serra-Picamal, V. Conte, M. Sales-Pardo, P. Roca-Cusachs, R. Gümèrà, X. Trepau, Regulation of cell cycle progression by cell–cell and cell–matrix forces. *Nat. Cell Biol.* **20**, 646–654 (2018).
- M. Baldassarre, I. Ayala, G. Beznoussenko, G. Giacchetti, L. M. Machesky, A. Luini, R. Buccione, Actin dynamics at sites of extracellular matrix degradation. *Eur. J. Cell Biol.* **85**, 1217–1231 (2006).
- M. F. Carlier, S. Shekhar, Global treadmill coordinates actin turnover and controls the size of actin networks. *Nat. Rev. Mol. Cell Biol.* **18**, 389–401 (2017).
- B. Pontes, P. Monzo, L. Gole, A.-L. Le Roux, A. J. Kosmalska, Z. Y. Tam, W. Luo, S. Kan, V. Giasnoff, P. Roca-Cusachs, L. Tucker-Kellogg, N. C. Gauthier, Membrane tension controls adhesion positioning at the leading edge of cells. *J. Cell Biol.* **216**, 2959–2977 (2017).
- C. Wang, H. J. Choi, S.-J. Kim, A. Desai, N. Lee, D. Kim, Y. Bae, K. Lee, Deconvolution of subcellular protrusion heterogeneity and the underlying actin regulator dynamics from live cell imaging. *Nat. Commun.* **9**, 1688 (2018).
- C.-H. Huang, M. Tang, C. Shi, P. A. Iglesias, P. N. Devreotes, An excitable signal integrator couples to an idling cytoskeletal oscillator to drive cell migration. *Nat. Cell Biol.* **15**, 1307–1316 (2013).
- S. Linder, C. Wiesner, Feel the force: Podosomes in mechanosensing. *Exp. Cell Res.* **343**, 67–72 (2016).
- K. M. Branch, D. Hoshino, A. M. Weaver, Adhesion rings surround invadopodia and promote maturation. *Biol. Open* **1**, 711–722 (2012).

Acknowledgments

Funding: This research was financially supported by the European Research Council under the European Union’s Horizon 2020 Framework Programme (ERC StG ABLASE, 640012), by BBSRC (BB/P027148/1), by an EPSRC Programme Grant (EP/P030017/1), the Department of Pathology, Albert Einstein College of Medicine, and by the EPSRC Doctoral Training Partnership (EP/N509759/1 and EP/L505079/1). J.E.S. is the Betty and Sheldon Feinberg Senior Faculty Scholar in Cancer (CA100324). **Author contributions:** E.D. conducted the experiments and analyzed the data with support from N.M.K. N.M.K. prepared ERISM substrates. N.M.K., J.E.S., and M.B.P. cosupervised the work. M.B.P. and M.C.G. conceived the project. E.D. and M.C.G. wrote the manuscript with input from all authors. M.C.G. supervised the project. **Competing interests:** The authors declare that they have no competing

interests. **Data and materials availability:** All data needed to evaluate the conclusions in the paper are present in the paper and/or the Supplementary Materials. Additional data related to this paper are available via <https://doi.org/10.17630/c039b84f-4bbe-4ec2-a2f9-59fc9a2c871f>. The UM-SCC-1 cell line was received via a material transfer agreement from T. Carey (University of Michigan). The UM-SCC-1 cell line and derivatives can be provided by J.E.S. and M.B.P. pending scientific review and a completed material transfer agreement with T. Carey. Requests for the UM-SCC-1 cell lines should be submitted to J.E.S. (jeffrey.segall@einsteinmed.org) or M.B.P. (Michael.Prystowsky@einstein.yu.edu).

Submitted 14 April 2019
Accepted 17 December 2019
Published 11 March 2020
10.1126/sciadv.aax6912

Citation: E. Dalaka, N. M. Kronenberg, P. Liehm, J. E. Segall, M. B. Prystowsky, M. C. Gather, Direct measurement of vertical forces shows correlation between mechanical activity and proteolytic ability of invadopodia. *Sci. Adv.* **6**, eaax6912 (2020).

Direct measurement of vertical forces shows correlation between mechanical activity and proteolytic ability of invadopodia

E. Dalaka, N. M. Kronenberg, P. Liehm, J. E. Segall, M. B. Prystowsky and M. C. Gather

Sci Adv 6 (11), eaax6912.
DOI: 10.1126/sciadv.aax6912

ARTICLE TOOLS

<http://advances.sciencemag.org/content/6/11/eaax6912>

SUPPLEMENTARY MATERIALS

<http://advances.sciencemag.org/content/suppl/2020/03/09/6.11.eaax6912.DC1>

REFERENCES

This article cites 49 articles, 10 of which you can access for free
<http://advances.sciencemag.org/content/6/11/eaax6912#BIBL>

PERMISSIONS

<http://www.sciencemag.org/help/reprints-and-permissions>

Use of this article is subject to the [Terms of Service](#)

Science Advances (ISSN 2375-2548) is published by the American Association for the Advancement of Science, 1200 New York Avenue NW, Washington, DC 20005. The title *Science Advances* is a registered trademark of AAAS.

Copyright © 2020 The Authors, some rights reserved; exclusive licensee American Association for the Advancement of Science. No claim to original U.S. Government Works. Distributed under a Creative Commons Attribution License 4.0 (CC BY).